Optimization of ground-state cooling of a mechanical mode using a three-level system

Neelesh Kumar Vij[1], Meenakshi Khosla[2], and Shilpi Gupta[1*]
[1] *Department of Electrical Engineering, Indian Institute of Technology Kanpur, Kanpur-208016, UP, India*
[2] *Department of Electrical and Computer Engineering, Cornell University, Ithaca, NY, 14850, USA*

We propose an optimization scheme for ground-state cooling of a mechanical mode by coupling to a general three-level system. We formulate the optimization scheme, using the master equation approach, over a broad range of system parameters including detunings, decay rates, coupling strengths, and pumping rate. We implement the optimization scheme on three physical systems: a colloidal quantum dot coupled to its confined phonon mode, a polariton coupled to a mechanical resonator mode, and a coupled-cavity system coupled to a mechanical resonator mode. These three physical systems span a broad range of mechanical mode frequencies, coupling rates, and decay rates. Our optimization scheme lowers the stead-state phonon number in all three cases by orders of magnitude. We also calculate the net cooling rate by estimating the phonon decay rate and show that the optimized system parameters also result in efficient cooling. The proposed optimization scheme can be readily extended to any generic driven three-level system coupled to a mechanical mode.

I. INTRODUCTION

Mechanical resonators have been an essential tool for precision metrology for a long time [1]. With the advancements in nanofabrication techniques, efforts are now oriented towards studying the quantum mechanical aspects of the mechanical resonators [1, 2]. Cooling a mechanical resonator to its motional ground state is of particular interest because of wide-ranging applications in the fields of quantum meteorology [3–7], information processing [8–12] and testing of quantum-classical boundary [13–16].

Coupling of the mechanical resonator with thermal bath results in heating and with dissipative channels results in cooling. Competing heating and cooling processes decide the extent of cooling of a mechanical resonator [17]. Therefore, the general approach to cool the resonator to its motional ground state is two fold: (a) reduce the heating rate by reducing the coupling of the mechanical resonator with thermal bath [18, 19] and (b) increase the cooling rate by engineering additional dissipative channels with hybrid quantum mechanical systems. Various approaches such as cooling with atoms or artificial atoms [20–26], dissipative optomechanical coupling [27–30], and interaction with a dark mode [31, 32] have been proposed and studied. To achieve maximum and efficient cooling, system parameters that are within experimental control need to be optimized. Many of these parameters depend on the physical realization of the dissipative channel and have been selectively studied in the literature; for example: detuning between the energy level of the dissipative channel and input laser [31, 33–37], coherent coupling strengths within the dissipative channel [31, 36–39] and the decay rates of the channel [38, 40]. However, simultaneous optimization of multiple system parameters is required to achieve maximum and efficient cooling.

Here, we propose a generalized framework to cool a mechanical mode using a three-level system. We formulate an optimization problem over various decay rates, pumping rates, detunings, and coupling strengths of the system using the master equation formalism. Our analysis covers all system parameters and can be mapped onto any generic three-level system that is coupled to a mechanical mode. We particularly show cooling of a mechanical mode coupled to three different systems — quantum dots, cavity polaritons, and coupled cavities — that can be modeled as three-level systems and can be easily integrated with micro- and nano-mechanical resonators. We show that optimization results in lowering of the steady-state phonon number by several orders of magnitude. For a measure of the efficiency of the cooling process, we estimate effective phonon decay rate that is equivalent to the net cooling rate. For maximum and efficient cooling, a small steady-state phonon number and a large effective phonon decay rate are required. We show that the optimized system parameters result in maximum and efficient cooling simultaneously.

The paper is organized as follows: In section (II) we describe our model for the three-level system coupled to a mechanical mode, show how the optimization problem for the minimum phonon number is inherent to the system, and discuss optimization of detunings and decay rates. In section (III) we subdivide the optimization problem into two categories based on the relative strength of the decay rates of the system and study them both analytically and numerically.

* corresponding author: ShilpiG@iitk.ac.in

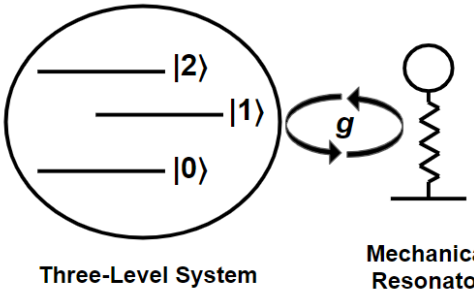

FIG. 1: Representation of a generic three-level system coupled to a mode of a mechanical resonator.

II. DESCRIPTION OF THE SYSTEM

A. Hamiltonian and master equation

We consider a mode of a mechanical resonator interacting with a generic three-level system, which comprises of the ground state $|0\rangle$, the first excited state $|1\rangle$, and the second excited state $|2\rangle$(Figure (1)). The three-level model can be realized in several systems including quantum dots [41], cavity polaritons [42], and coupled cavity systems [37] — we discuss each one of them in detail later. The phonon mode is coupled to the two excited states of the three-level system with strength g. We also consider a coherent pump of strength Ω and frequency ω_p between the states $|0\rangle$ and $|1\rangle$. The Hamiltonian accounting for all the interactions, under the rotating wave approximation, is following:

$$\begin{aligned}\mathbf{H}_{\mathrm{s}} &= \omega_1\sigma_{11} + \omega_2\sigma_{22} + \omega_m b^\dagger b + g(\sigma_{12}b^\dagger + \sigma_{21}b) \\ &\quad + \Omega\big(\sigma_{01}e^{i\omega_p t} + \sigma_{10}e^{-i\omega_p t}\big)\end{aligned} \tag{1}$$

where ω_1 and ω_2 are frequencies of the states $|1\rangle$ and $|2\rangle$ respectively, and ω_m is frequency of the phonon mode. The operator $\sigma_{ij} = |i\rangle\langle j|$ represents population operator when $i = j$ and dipole operator when $i \neq j$. The annihilation (creation) operator for the phonon mode is b ($b^\dagger$). We set the energy of the ground state of the three-level system to zero. To remove the time-dependent terms, we move to a suitable rotated frame to obtain the rotated Hamiltonian (see derivation in Appendix (A)):

$$\begin{aligned}\mathbf{H}_{\mathrm{rot}} &= \Delta_1\sigma_{11} + (\Delta_1 + \Delta_2)\sigma_{22} + \Omega(\sigma_{01} + \sigma_{10}) \\ &\quad + g(\sigma_{12}b^\dagger + \sigma_{21}b)\end{aligned} \tag{2}$$

where $\Delta_1 = \omega_1 - \omega_p$ and $\Delta_2 = \omega_2 - \omega_1 - \omega_m$ are the detunings. To analyse the complete dynamics of the system, we use the Lindblad master equation for the combined density operator ρ under the Born-Markov approximation:

$$\begin{aligned}\frac{d\rho}{dt} &= i[\rho, \mathbf{H}_{\mathrm{rot}}] + \gamma_1\mathcal{L}[\sigma_{01}]\rho + \gamma_2\mathcal{L}[\sigma_{02}]\rho \\ &\quad + \gamma(n_{th}+1)\mathcal{L}[b]\rho + \gamma n_{th}\mathcal{L}[b^\dagger]\rho\end{aligned} \tag{3}$$

Here, $\mathcal{L}[\mathcal{O}]\rho = \mathcal{O}\rho\mathcal{O}^\dagger - \frac{1}{2}(\mathcal{O}\mathcal{O}^\dagger\rho + \rho\mathcal{O}\mathcal{O}^\dagger)$, γ_1 and γ_2 are the decay rates of $|1\rangle$ and $|2\rangle$ respectively, γ is the decay rate of phonon mode, and $n_{th} = 1/e^{(\hbar\omega_m/k_BT)}$ is the phonon number in thermal equilibrium at temperature T and energy $\hbar\omega_m$. The last two terms in equation 3 account for the coupling of the mechanical mode with the reservoir held at a constant temperature T. We will use Eqs. 2-3 in the next section for setting up the optimization problem to achieve the minimum phonon number.

B. Deriving the optimization problem

We set up the optimization problem for achieving the minimum phonon number by writing the Heisenberg operator equations for the expectation value of the phonon number operator ($b^\dagger b$) and the population operator of the second excited state (σ_{22}) using Eqs. 2-3:

$$\frac{d\langle b^\dagger b\rangle}{dt} = ig\langle\sigma_{21}b - \sigma_{12}b^\dagger\rangle + \gamma\big(n_{th} - \langle b^\dagger b\rangle\big) \tag{4}$$

$$\frac{d\langle\sigma_{22}\rangle}{dt} = ig\langle\sigma_{12}b^\dagger - \sigma_{21}b\rangle - \gamma_2\langle\sigma_{22}\rangle \tag{5}$$

Solving in steady state gives:

$$\langle b^\dagger b\rangle_s = n_{th} - \frac{\gamma_2}{\gamma}\langle\sigma_{22}\rangle_s \tag{6}$$

where the subscript denotes the expectation values calculated in steady state. The above equation brings out the inherent optimization problem present in the combined system. To minimize the steady-state phonon number, we need to maximize the term $\gamma_2\langle\sigma_{22}\rangle_s$. However, as we increase γ_2, the steady-state population of the state $|2\rangle$, represented by $\langle\sigma_{22}\rangle_s$, decreases and vice-versa. Thus, an optimal value of γ_2 exists, which leads to a minimum phonon number. The optimization also depends on the other parameters of the system (decay rates, detunings, coupling strength and pumping strength) that come into play via the expression of $\langle\sigma_{22}\rangle_s$. Next, we analyze the role of each of these parameters in minimizing the steady-state phonon number.

Depending on the platform in which the three-level system is realized, the coupling strengths and the decay rates can range from MHz - GHz [33, 37, 41]. For this section, we set $g = 5$ GHz, $\omega_2 - \omega_1 = 0.5$ meV, and an initial temperature of 50 K. We also define a figure of merit for cooling of the mechanical mode as $\mathcal{F} = \langle b^\dagger b\rangle_s / n_{th}$, which needs to be minimized [40].

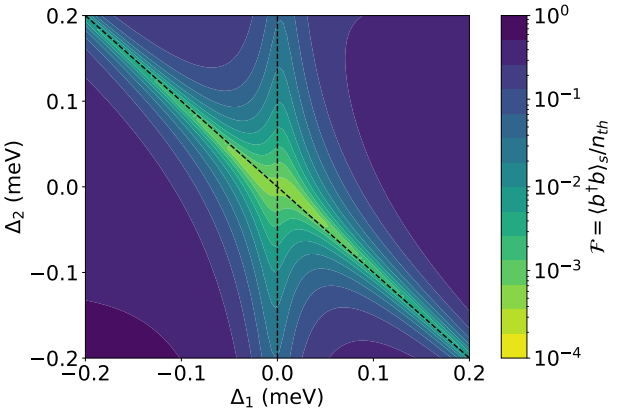

FIG. 2: Variation of $\mathcal{F} = \langle b^\dagger b \rangle_s / n_{th}$ with detunings Δ_1 and Δ_2. Here, $g = 5$ GHz, $\omega_2 - \omega_1 = 0.5$ meV, $\Omega = \gamma_2 = g/2, \gamma_1 = 10^{-1}g, \gamma = 10^{-4}g$ and an initial temperature of 50 K.

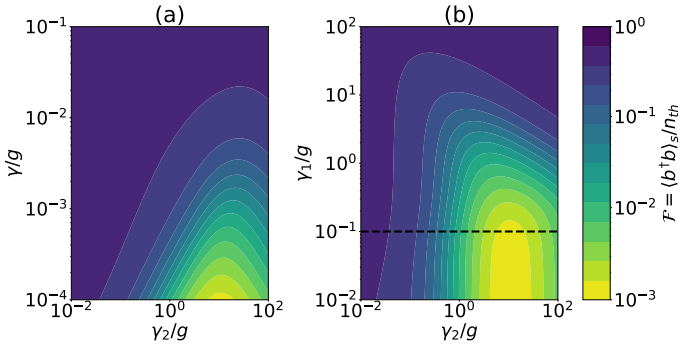

FIG. 3: Variation of $\mathcal{F}$ with (a) phonon decay rate γ and decay rate of the second excited state γ_2 (b) decay rate of the first excited state γ_1 and the second excited state γ_2. The black dashed horizontal line denotes $\gamma_1 = \Omega = 10^{-1}g$. Here, $g = 5$ GHz, $\Delta_1 = \Delta_2 = 0$, $\omega_2 - \omega_1 = 0.5$ meV, $\gamma_2 = g/2, \Omega = \gamma_1 = 10^{-1}g, \gamma = 10^{-4}g$ and an initial temperature of 50 K.

1. *Effect of Detuning*

First we analyze the effect of the detunings Δ_1 and Δ_2 on the figure of merit $\mathcal{F}$. For this calculation, we fix $\gamma_2 = g/2, \Omega = \gamma_1 = 10^{-1}g, \gamma = 10^{-4}g$. Using the quantum optics toolbox QuTip [43], we calculate variation of $\mathcal{F}$ with detunings Δ_1 and Δ_2 (Figure (2)). As expected, for highly off-resonant interactions, $\mathcal{F} \approx 1$, implying negligible cooling. Minimization of the figure of merit is achieved along the dashed lines $\Delta_1 = 0$, which represents resonance between the pump and the $|0\rangle$ - $|1\rangle$ transition, and $\Delta_2 = -\Delta_1$, which represents resonance between the mechanical mode and the $|1\rangle$ - $|2\rangle$ transition. Global minimization of $\mathcal{F}$ happens when both $\Delta_1 = 0$ and $\Delta_2 = 0$. However, we note that even when the phonon mode is off-resonant with the $|1\rangle$ - $|2\rangle$ transition (i.e. $\Delta_2 \neq 0$), a local minimization of $\mathcal{F}$ can be achieved by tuning the frequency of the coherent pump such that $\Delta_1 = -\Delta_2$. This offers a convenient way to minimize the phonon number in the case of off-resonant phonon coupling.

The optimal values of the detunings Δ_1 and Δ_2 are also mandated by the coherent coupling strengths g and Ω. If either g or Ω dominates the other rates, the minimum $\mathcal{F}$ is achieved for non-zero detuning values (Appendix (B)). Since the pumping strength Ω is a control parameter in experiments, we choose it to be of the same order as g and thus, set $\Delta_1 = \Delta_2 = 0$ in further calculations.

2. *Effect of Decay Rates*

Next, we analyze the effect of the decay rates on the figure of merit $\mathcal{F}$. Figure 3a plots the variation of $\mathcal{F}$ as a function of the phonon decay rate γ and the decay rate of the second excited state γ_2 for $\Omega = \gamma_1 = 10^{-1}g$. We make the following observations:

1. $\mathcal{F}$ decreases as the phonon decay rate γ decreases. In other words, $\mathcal{F}$ is minimized when the interaction of the mechanical mode with the reservoir is minimized. Thus, for further calculations, we assume that $\gamma_2 \gg \gamma$. This condition ensures minimum heating rate of the mechanical mode.

2. There exists an optimal γ_2 that minimizes $\mathcal{F}$. This is consistent with our explanation presented in the previous section, using Eq. 6, that there exists an optimal γ_2 which minimizes the steady state phonon number.

Figure 3b shows the variation of $\mathcal{F}$ with γ_1 and γ_2 for $\Omega = 10^{-1}g$ and $\gamma = 10^{-4}g$. Consistent with Figure 3a, Figure 3b exhibits the same optimal γ_2 for $\gamma_1 < \Omega$. For $\gamma_1 > \Omega$ (indicated by the black dashed line), a large decoherence is induced between the states $|0\rangle$ and $|1\rangle$ because of which the optimal γ_2 decreases as γ_1 increases beyond Ω. This is indicated by the gradient in $\mathcal{F}$ in the upper left region of the plot. For the cases when $\gamma_1 > \Omega$ and γ_2 is greater than its optimal value, decoherence dominates which leads to $\mathcal{F} \approx 1$ as depicted in the upper right region of the plot.

The above discussion gives us a broad set of conditions for the system parameters which lead to minimization of the phonon number: (i) $\Omega \approx g$ with $\Delta_1 = -\Delta_2$, (ii) $\gamma \ll \gamma_2$, (iii) $\gamma_1 < \Omega$, and (iv) $\gamma_2 \geq \gamma_1$. Fixing the first three conditions, we divide the last condition into two regimes: (1)$\gamma_1 \ll \gamma_2$ and $\gamma_1 = \gamma_2$ and perform optimization. In the next section, we analytically formulate the cooling optimization problem for these two regimes and discuss the outcomes for physical systems that exemplify them.

III. COOLING OPTIMIZATION FOR DIFFERENT REGIMES

In this section, we derive analytical models for two regimes of decay rates by restricting the excitations of the mechanical resonator mode to one. We compare the results of our analytical model with numerical simulations performed for a larger basis of phonon mode and show that the restriction is valid under the considered temperature range.

A. $\gamma_1 \ll \gamma_2$

We derive the rate equations for the density matrix elements of the combined state basis (see Appendix (C)) and solve them, under the approximation $\gamma_1 \ll \gamma_2$, to get the steady state phonon number as

$$\langle b^\dagger b\rangle_s \approx \frac{n_{th}}{(2+3n_{th})+\gamma_2/\left[\gamma\left(\frac{\gamma_2^2}{2g^2}+\frac{2\Omega^2}{g^2}\right)\right]} + \frac{n_{th}}{(2+3n_{th})+\gamma_2/\left[\gamma\left(\frac{\gamma_2^2}{2g^2}+\frac{2\Omega^2}{g^2}+\frac{g^2}{2\Omega^2}-1\right)\right]} \tag{7}$$

To set values of the parameters for this regime, we consider a system comprising of a cadmium selenide colloidal quantum dot coupled to its confined phonon mode via deformation potential. For temperatures < 20 K, the colloidal quantum dot can be approximated as a three-level system with first and second excited states $|1\rangle$ and $|2\rangle$ being dark and bright states, respectively [41, 44]. The dark state of the colloidal quantum dot has a lifetime of ~ 1 ms and the bright state has a lifetime of ~ 10 ns. Therefore, this quantum dot - phonon system exemplifies the regime of $\gamma_2 \gg \gamma_1$. To facilitate coherent pumping to the dark state, two-photon absorption techniques can be used [45]. The decay rate of the bright state can be altered via Purcell enhancement by coupling to an optical cavity. Purcell factors upto 10^4 have been achieved using appropriate cavity geometry [46, 47]. Consistent with the literature, we set the following values for the system parameters: $\omega_m = 1$ meV, $g = 20$ GHz, $\gamma_1 = 10^{-6}$ GHz, $\gamma = 10^{-3}$ GHz and the initial temperature $= 17$ K which corresponds to $n_{th} = 1$, for further calculations in this subsection.

The strength of coherent pumping Ω and the decay rate of the bright state γ_2 are the control parameters in this system. Therefore, we plot the figure of merit of minimization of phonon number $\mathcal{F}$ as a function of Ω and γ_2 using Eq. (7) in Figure 4a. We observe that $\mathcal{F}$ minimizes for optimal values of Ω and γ_2, as discussed in Section II B. We also calculate $\mathcal{F}$ exactly by numerically solving the master equation (Eq (3)) using the quantum optics toolbox without making the approximation to restrict the mechanical mode excitations, that we used in arriving at Eq (7) (Figure 4b). We note that the theoretical and simulation results are in good agreement, justifying that the higher order phonon excitations are sparsely populated and can thus be neglected. The approximation however breaks down if the rate of bulk phonon decaying into the system ($= \gamma n_{th}$) is comparable to other rates in the system. This can happen when either n_{th}, governed by the initial temperature, or γ, governed by the quality factor of the mechanical resonator mode, is large

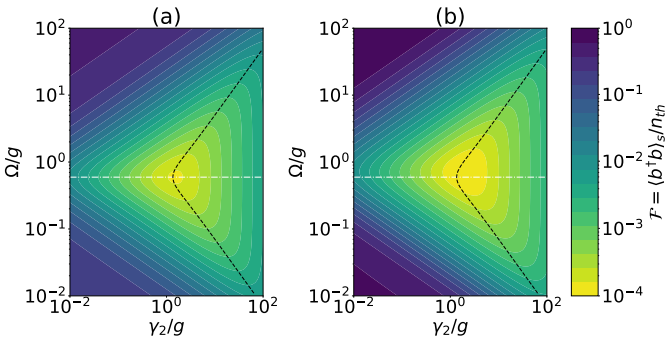

FIG. 4: **Regime** $\gamma_1 \ll \gamma_2$: Variation of $\mathcal{F}$ with pumping strength Ω and decay rate of second excited state γ_2 as per (a) theoretical result Eq (7) and (b) simulation results. The white dot-dashed line and the black dashed curve represent the optimal parameters Ω_o and γ_{2_o} respectively as derived in Eq (8). Here, $\omega_m = 1$ meV, $g = 20$ GHz, $\gamma_1 = 10^{-6}$ GHz, $\gamma = 10^{-3}$ GHz and the initial temperature $= 17$ K.

We further calculate analytical expressions for optimum Ω and γ_2 that minimize the steady-state phonon number, and thus minimize $\mathcal{F}$. Since $\gamma_2 \gg \gamma$, we neglect $(2+3n_{th})$ from the denominators in Eq. (7) and arrive at the expressions for optimal pumping strength Ω_o and optimal decay rate of the bright state γ_{2o}:

$$\Omega_o = \frac{g}{2^{3/4}} \approx 0.6g$$
$$\gamma_{2_o} = \sqrt{4\Omega^2 + \frac{g^4}{2\Omega^2} - g^2} \tag{8}$$

We plot Ω_o/g as a white dot-dashed line and γ_{2_o}/g as a black dashed curve in Figure 4. We observe that the optimal pumping strength is a function of only the coupling strength while the optimal decay rate of the bright state is a function of both the pumping strength and the coupling strength. The dependence of γ_{2_o} on Ω and g arises because the two coherent processes compete with the incoherent process for population transfer from the second excited state. The optimal pumping strength $\Omega_o \approx 0.6g$ obtained analytically differs marginally from the optimal pumping strength obtained from simulation $\approx 0.7g$. We ascribe this difference to the approximations made in our analytical model. As discussed in [40], critical coupling $\gamma_2 \gtrsim g$ is necessary for a small $\mathcal{F}$, as can also be seen in Figure 4.

Cooling efficiency: With the optimization in place for this regime, we now estimate the efficiency of the cooling process by calculating the effective phonon decay

rate (γ_{eff}). We plot the variation of phonon number with time, using the quantum optics toolbox, and fit an exponentially decaying function of the form $f(t) = (n_{th} - \langle b^\dagger b\rangle_s)e^{-\gamma_{\text{eff}}t} + \langle b^\dagger b\rangle_s$ to it (Figures 5a-f). Repeating the procedure of fitting and extracting γ_{eff} over a range of values of Ω and γ_2, we plot dependence of $\gamma_{\text{eff}}/\omega_m$ on Ω and γ_2 (Figure 5g). We observe that the same range of Ω and γ_2 maximize γ_{eff} (Figure 5g) and minimize $\mathcal{F}$ (Figure 4). To demonstrate this point clearly, we plot the ratio of $\gamma_{\text{eff}}/\omega_m$ to $\mathcal{F}$ in Figure 5h. Large value of this ratio within the optimized ranges of Ω and γ_2 implies that our optimization process simultaneously ensures maximum and efficient cooling of the mechanical resonator mode. The optimal parameters derived for this regime are summarized in Table (I).

B. $\gamma_1 = \gamma_2$

For $\gamma_1 = \gamma_2$ regime , we consider a single mode cavity mode strongly coupled to a two-level system (TLS), forming polaritons, that in turn couple to a mode of a mechanical resonator. The Hamiltonian for the system takes the following form (See Appendix (D) for details) [42]:

$$\begin{aligned}\mathbf{H} &= \omega_1\sigma_{11} + \omega_2\sigma_{22} + \omega_m b^\dagger b \\ &+ \frac{g}{2}\sin(2\theta)(\sigma_{21}b + \sigma_{12}b^\dagger) \\ &+ \frac{g}{2}\cos(2\theta)(\sigma_{11} - \sigma_{22})(b + b^\dagger) \\ &+ \Omega\big(\sigma_{01}e^{i\omega_p t} + \sigma_{10}e^{-i\omega_p t}\big)\end{aligned} \tag{9}$$

where $|1\rangle$ and $|2\rangle$ are the polariton states of the hybrid system with energies ω_1 and ω_2 respectively, $|0\rangle$ is the ground state, G and Δ are the coupling strength and detuning between the TLS and the cavity mode such that $\tan(2\theta) = 2G/\Delta$, Ω is the coherent pumping strength, and g is the coupling strength between the polariton states and the mechanical mode of energy ω_m. By writing the Hamiltonian in the polariton-phonon basis, two different couplings can be identified [48]. First, the term proportional to $\sin(2\theta)(\sigma_{21}b + \sigma_{12}b^\dagger)$ is the usual Jaynes-Cummings coupling and is responsible for coherent population exchange between the polariton states and the mechanical resonator mode. Second, the term proportional to $\cos(2\theta)(\sigma_{11} - \sigma_{22})(b + b^\dagger)$ is responsible for the dispersive coupling between the polariton states and the mechanical resonator mode. For $2\theta \neq \pi/2$, the dispersive coupling competes with the Jaynes-Cummings coupling that is responsible for cooling, and adversely affects the cooling of the mechanical mode. Therefore, we choose $2\theta = \pi/2$ such that the dispersive coupling goes to zero and the Hamiltonian resembles to that in Eq (2). To achieve $2\theta = \pi/2$, the detuning between the TLS and cavity mode (Δ) must be zero, and thus the decay rates of the polariton states $|1\rangle$ and $|2\rangle$ will be equal (See Appendix (D) for details). Therefore, $\gamma_1 = \gamma_2$ and we use the latter symbol to denote the decay rates. We solve the rate equations for the density matrix elements in the combined state basis (Appendix (C)) to obtain the expression for the steady state phonon number under the condition $\gamma_1 = \gamma_2$ (Appendix (E)).

We set $G = 20$ GHz, cavity decay $\kappa = 2.5$ GHz, $g = 0.05G, \omega_m = 2G, Q_m = \omega_m/\gamma = 10^6$, and an initial temperature of 20 K corresponding to $n_{th} = 10$ [33]. In this system, the strength of coherent pumping Ω and the decay rate γ_2 are the control parameters. The decay rate γ_2 depends on the cavity decay rate (Appendix (D), Eq. D6), which can be controlled by appropriate design and fabrication of the cavity. Therefore, we plot the figure of merit of minimization of phonon number $\mathcal{F}$ as a function of Ω and γ_2 using Eq. E1 in Figure 6a and by numerically solving the master equation (Eq. 3) using quantum optics toolbox, without making any approximations, in Figure 6b. We observe that the theoretical and the simulation results are in good agreement, and $\mathcal{F}$ minimizes for optimal values of Ω and γ_2, just like in the previous regime. Obtaining analyical expressions for optimal Ω and γ_2 is difficult because of sheer complexity of the expression of the steady state phonon number (Eq. E1). However, they can be obtained by fitting the calculated data.

Cooling efficiency: With the optimization in place, we now proceed to calculate the effective decay rate for the phonon mode to get a measure of the efficiency of the cooling process. Figures 7a-f show variation of phonon number with time for different values of Ω and γ_2, and the associated exponential fits. Figures 7g shows dependence of $\gamma_{\text{eff}}/\omega_m$ over a range of values of Ω and γ_2. We also plot the ratio of $\gamma_{\text{eff}}/\omega_m$ to $\mathcal{F}$ in Figure 7h that shows that the optimization ensures maximum and efficient cooling simultaneously.

Another system that satisfies the condition $\gamma_1 = \gamma_2$ is a system of coupled cavities interacting with a mechanical resonator mode. The system has been experimentally realized in a different context using coupled torroidal cavities out of which one supports a mechanical mode [49]. Following the optimization method outlined in this subsection, we show ground state cooling by optimizing Ω and γ_2 for this system as well (see Appendix (F)).

IV. CONCLUSION AND DISCUSSION

We proposed cooling of a mechanical resonator mode using a general three-level system. We formulated an optimization problem, using the master equation approach, over a broad range of system parameters including detuning, decay rates, coupling strengths, and pumping rate. Through particular examples of three physical systems with differing mechanical mode frequencies, coupling strengths, and decay rates — a colloidal quantum

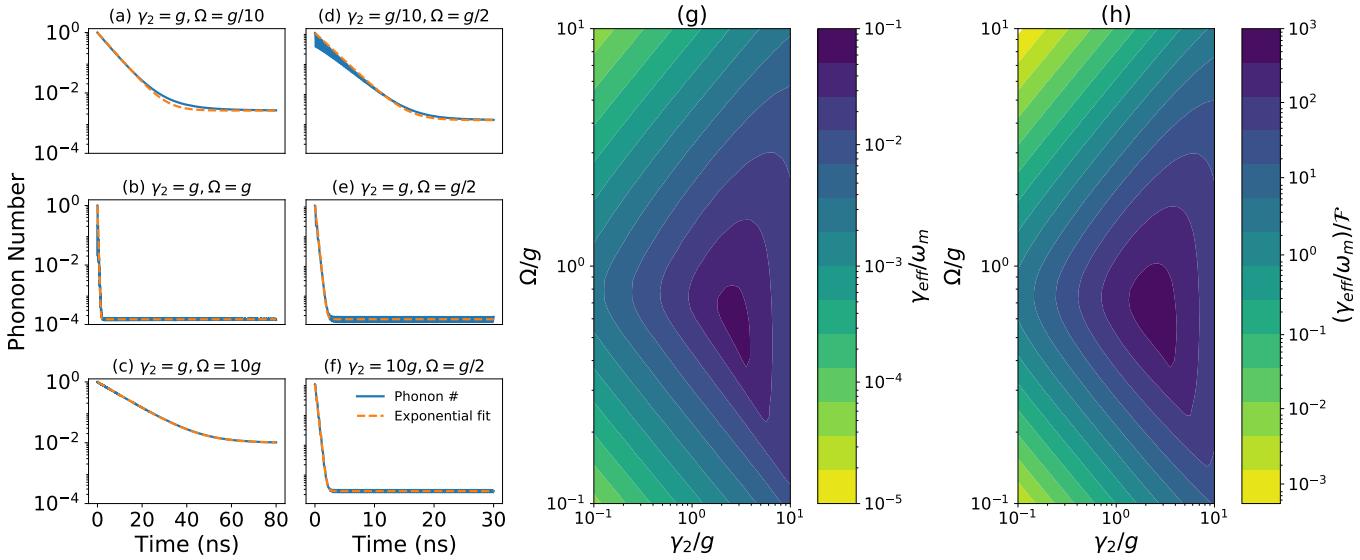

FIG. 5: **Regime** $\gamma_1 \ll \gamma_2$: (a)-(f) Time-dependent decay of phonon number and the exponential fit for various values of Ω and γ_2. (g) $\gamma_{\text{eff}}/\omega_m$ over a range of values of Ω and γ_2. (h) $(\gamma_{\text{eff}}/\omega_m)/\mathcal{F}$ over a range of values of Ω and γ_2.

TABLE I: Optimal parameters for $\gamma_1 \ll \gamma_2$

Parameter	**Can be Tuned?**	**Optimal Value**
$\Delta_1 (= \omega_1 - \omega_p)$	Yes	Set to $-\Delta_2$
$\Delta_2 (= \omega_2 - \omega_1 - \omega_m)$	No	Is set to 0
Coupling Strength g	No	Fixed for the system but should be as large as possible
Coherent pumping strength Ω	Yes	$0.6g$
Phonon decay rate γ	No	Fixed for the system but should be as small as possible.
Decay rate of dark state γ_1	No	Fixed for the system
Decay rate of bright state γ_2	Yes	$\sqrt{4\Omega^2 + g^4/2\Omega^2 - g^2}$

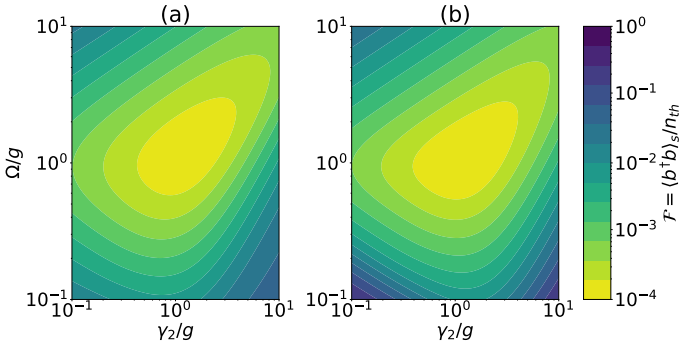

FIG. 6: **Regime** $\gamma_1 = \gamma_2$: Variation of $\mathcal{F}$ with Ω and γ_2 as per (a) theoretical result Eq E1 and (b) simulation results. Here, $G = 20$ GHz, $g = 0.05G, \omega_m = 2G, Q_m = \omega_m/\gamma = 10^6$, and an initial temperature of 20 K corresponding to $n_{th} = 10$.

dot coupled to its confined phonon mode, a polariton coupled to a mechanical resonator mode, and a coupled-cavity system coupled to a mechanical resonator — we showed that our model could be adapted to any three-level system coupled to a mechanical mode. In all the three systems, ground-state cooling was achieved by optimizing the system parameters. We also calculated the cooling efficiency by estimating the rate of phonon decay, and showed that the optimized system parameters result in both maximum and efficient cooling.

While some previous works have looked at selective optimization of system parameters, our model provides optimization over a broad range of multiple parameters. For example, our model is a generalization to the model presented in [40] where the three-level system was effectively reduced to a two-level system on application of a strong incoherent pump to the first excited state. Replacing the coherent pump with an incoherent pump, our model reproduces the result of [40] for the case of single atom, giving the optimal decay rate $\gamma_{2_o} = 2g$.

ACKNOWLEDGMENTS

We acknowledge funding support from SERB (SB/S2/RJN-134/2014, EMR/2016/007113). We thank Harshawardhan Wanare, Saikat Ghosh, and Shruti Shukla for insightful discussions.

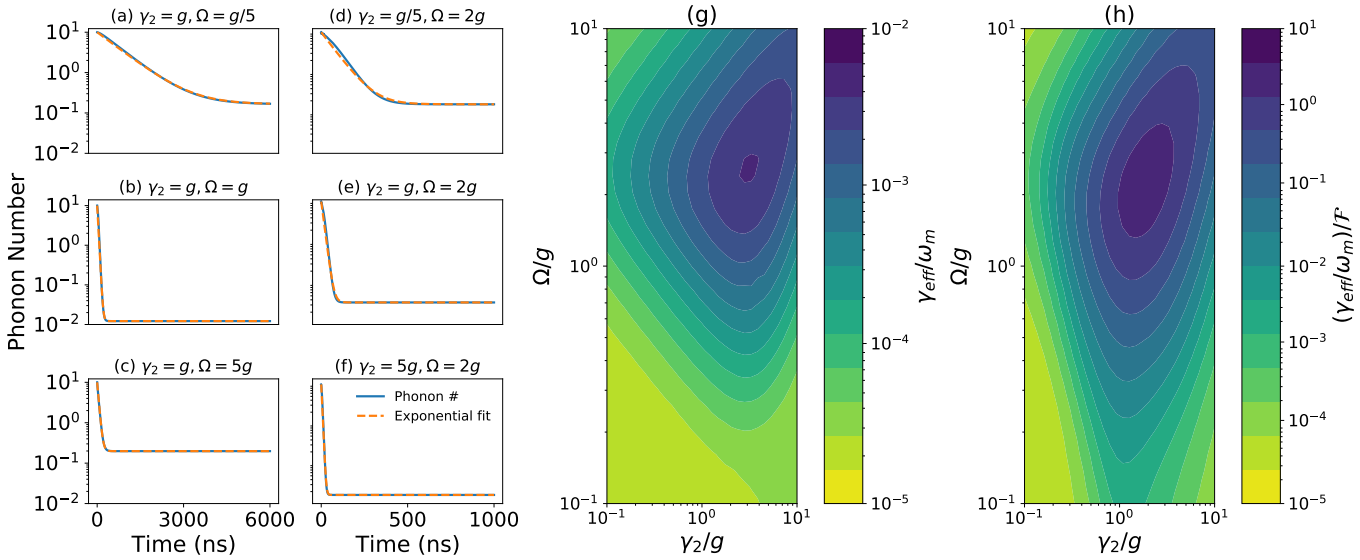

FIG. 7: **Regime** $\gamma_1 = \gamma_2$: (a)-(f) Time dependent phonon number and the exponential fit on top of it for various values of Ω and γ_2. (g) $\gamma_{\text{eff}}/\omega_m$ over a range of values of Ω and γ_2. (h) $(\gamma_{\text{eff}}/\omega_m)/\mathcal{F}$ over a range of values of Ω and γ_2.

TABLE II: Optimal parameters for $\gamma_2 = \gamma_1$

Parameter	**Can be Tuned?**	**Optimal Value**
$\Delta_1 (= \omega_1 - \omega_p)$	Yes	Set to $-\Delta_2$
$\Delta_2 (= \omega_2 - \omega_1 - \omega_m)$	No	Is set to 0
Coupling Strength g	No	Fixed for the system but should be as large as possible
Coherent pumping strength Ω	Yes	can be obtained numerically (Figure 6)
Phonon decay rate γ	No	Fixed for the system but should be as small as possible.
Decay rate of first hybrid state γ_1	Yes	can be obtained numerically (Figure 6)
Decay rate of second hybrid state γ_2	Yes	can be obtained numerically (Figure 6)

Appendix A: Conversion of Hamiltonian to a Rotated frame

Using a unitary transformation, defined by $\mathbf{U} = e^{-i\mathbf{H_o}t/\hbar}$, we transform our system Hamiltonian H_s to $\mathbf{H}_{\text{rot}} = \mathbf{U}^\dagger \mathbf{H} \mathbf{U} - \mathbf{H_o}$ into a new rotating frame of reference [50]. We choose $\mathbf{H_o} = \alpha\sigma_{11} + \beta\sigma_{22} + \zeta b^\dagger b$ and determine $\alpha = \omega_p, \beta = \omega_p + \omega_m$, and $\zeta = \omega_m$ such that the rotated Hamiltonian takes the following time-independent form (Eq. 2):

$$\mathbf{H}_{\text{rot}} = \Delta_1\sigma_{11} + (\Delta_1 + \Delta_2)\sigma_{22} + g(\sigma_{12}b^\dagger + \sigma_{21}b) + \Omega(\sigma_{01} + \sigma_{10}) \tag{A1}$$

where $\Delta_1 = \omega_1 - \omega_p$ and $\Delta_2 = \omega_2 - \omega_1 - \omega_m$.

Appendix B: Variation of $\mathcal{F}$ with detunings

Here, we discuss variation of $\mathcal{F}$ with detunings Δ_1 and Δ_2 for two other cases: $\Omega \gg g$ and $g \gg \Omega$. In these cases, one coherent process dominates the other and thus the detunings between the energy levels are modified. To analyse these modified detunings, we diagonalize the rotated hamiltonian with respect to the dominant coherent process, neglecting the other. For resonant interaction, the modified detunings should be set to zero to give the condition for optimal detuning.

When $\Omega \gg g$, the eigenenergies of the rotated hamiltonian, neglecting the phonon coupling term are: $\omega_\pm = -\Delta_1/2 \pm \sqrt{\Delta_1^2/4 + \Omega^2}, \omega_2 = \Delta_1 + \Delta_2$. The second excited state $|2\rangle$ now couples to both the dressed states. The modified detunings thus are $\Delta_\pm = \Delta_2 + \Delta_1/2 \pm \sqrt{\Delta_1^2/4 + \Omega^2}$. Setting them to zero gives the optimal detuning condition: $\Delta_2 = -\Delta_1/2 \pm \sqrt{\Delta_1^2/4 + \Omega^2}$.

For the case $g \gg \Omega$, diagonalizing the rotated hamiltonian, neglecting the pumping term gives the following eigenenergies: $\omega_o = 0, \omega_\pm = \Delta_1 + \Delta_2/2 \pm \sqrt{\Delta_2^2/4 + g^2}$. The modified detunings $\Delta_\pm = \Delta_1 + \Delta_2/2 \pm \sqrt{\Delta_2^2/4 + g^2}$ when set to zero give the optimal detuning condition: $\Delta_1 = -\Delta_2/2 \pm \sqrt{\Delta_2^2/4 + g^2}$.

Using quantum optics toolbox, we simulate the varia-

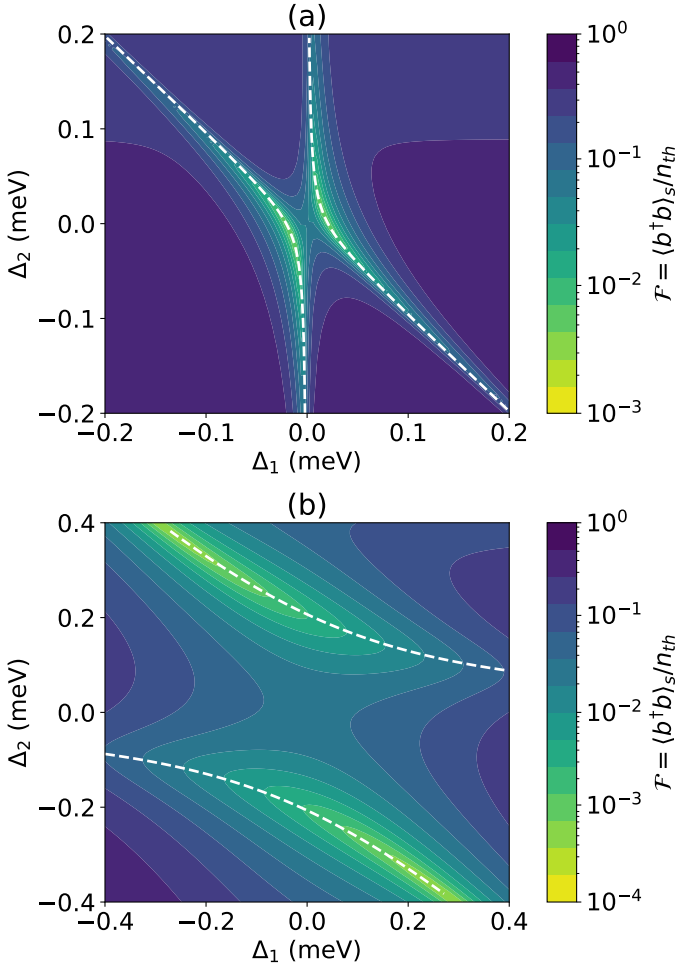

FIG. 8: Variation of $\mathcal{F} = \langle b^\dagger b \rangle / n_{th}$ with detunings Δ_1 and Δ_2 for two different regimes. (a) $\Omega = 10^{-1}g$. The white dashed curves represent the analytically derived optimal detuning expressions $\Delta_1 = -\Delta_2/2 \pm \sqrt{\Delta_2^2/4 + g^2}$. (b) $\Omega = 10g$. The white dashed curves represent the analytically derived optimal detuning expressions $\Delta_2 = -\Delta_1/2 \pm \sqrt{\Delta_1^2/4 + \Omega^2}$. Here, $g = 5$ GHz, $\omega_2 - \omega_1 = 0.5$ meV, $\gamma_2 = g/2, \gamma_1 = 10^{-1}g, \gamma = 10^{-4}g$ and an initial temperature of 50 K.

tion in the figure of merit $\mathcal{F}$ with Δ_1 and Δ_2 in Figure 8. We set $\omega_2 - \omega_1 = 0.5$ meV, $\gamma_2 = g/2, \gamma_1 = 10^{-1}g, \gamma = 10^{-4}g$ and an initial temperature of 50 K. We also plot the analytically derived expressions of optimal detuning as white dashed curves. For $g > \Omega$ case, we set $g = 5$ GHz and $\Omega = 10^{-1}g$ and for $\Omega \gg g$ case, we set $g = 5$ GHz and $\Omega = 10g$. Both these cases also show that local minimization of $\mathcal{F}$ is achievable in non-resonant system by tuning the pump frequency.

Appendix C: Rate equations for density matrix elements

We denote the combined states of the three-level system and the mechanical resonator mode by $|i, j\rangle$ where indices $i \in [0, 1, 2]$ and $j \in [0, 1]$ correspond to the three-level system and the mechanical resonator, respectively (Figure 9). For brevity, we label the combined state basis as $|a\rangle, |b\rangle, .., |e\rangle$ as depicted in Figure 9 by the labels on the left.

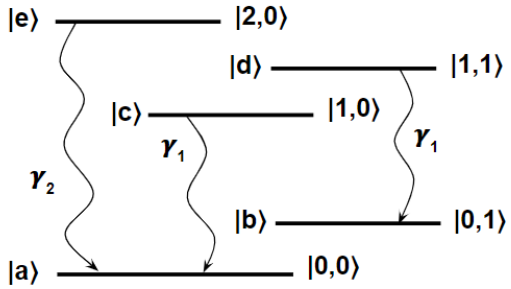

FIG. 9: Combined states for the three-level system and mechanical resonator mode of the form $|i, j\rangle$ where index i and j corresponds to the three-level system and the mechanical resonator mode respectively.

The rate equation for any element of the density matrix can be derived by taking the respective components projections on both sides of the master equation. The following elements of the density matrix are needed to completely describe the dynamics of the combined system:

$$
\begin{aligned}
\frac{d\rho_{bb}}{dt} &= i\Omega(\rho_{bd} - \rho_{db}) + \gamma n_{th}\rho_{aa} - \gamma(n_{th}+1)\rho_{bb} + \gamma_1\rho_{dd} \\
\frac{d\rho_{cc}}{dt} &= i\Omega(\rho_{ca} - \rho_{ac}) + \gamma(n_{th}+1)\rho_{dd} - \gamma n_{th}\rho_{cc} - \gamma_1\rho_{cc} \\
\frac{d\rho_{dd}}{dt} &= ig(\rho_{de} - \rho_{ed}) + i\Omega(\rho_{db} - \rho_{bd}) + \gamma n_{th}\rho_{cc} \\
&\quad - \gamma(n_{th}+1)\rho_{dd} - \gamma_1\rho_{dd} \\
\frac{d\rho_{ee}}{dt} &= ig(\rho_{ed} - \rho_{de}) - \gamma_2\rho_{dd} \\
\frac{d\rho_{de}}{dt} &= ig(\rho_{dd} - \rho_{dd}) + i\Omega\rho_{eb} - \frac{\gamma_1+\gamma_2}{2}\rho_{ed} \\
\frac{d\rho_{db}}{dt} &= -ig\rho_{eb} + i\Omega(\rho_{dd} - \rho_{bb}) + \gamma n_{th}\rho_{ca} \\
&\quad - \gamma(n_{th}+1)\rho_{db} - \frac{\gamma_1}{2}\rho_{db} \\
\frac{d\rho_{ca}}{dt} &= i\Omega(\rho_{cc} - \rho_{aa}) + \gamma(n_{th}+1)\rho_{db} - \frac{\gamma_1}{2}\rho_{ca} \\
\frac{d\rho_{eb}}{dt} &= -ig\rho_{eb} + i\Omega\rho_{ed} - \frac{\gamma_1+\gamma_2}{2}\rho_{eb}
\end{aligned}
\tag{C1}
$$

In steady state, setting the time derivative to zero, the above equation can be solved to derive the expression for

the steady state phonon number, which is $= \rho_{bb} + \rho_{dd}$.

Appendix D: Hamiltonian of a TLS coupled to an optical cavity mode and a mechanical resonator

The Hamiltonian for a a single mode cavity mode strongly coupled to a two-level system (TLS), forming polaritons, that in turn couple to a mode of a mechanical resonator is given by

$$\begin{aligned}\mathbf{H}_{\rm s} = &\underbrace{\omega_c a^\dagger a + \omega_a \sigma_{\alpha\alpha} + \hbar G(\sigma_{\beta\alpha} a^\dagger + \sigma_{\alpha\beta} a)}_{\mathbf{H}_{\rm JC}} \\ &+ \omega_m b^\dagger b + g a^\dagger a (b^\dagger + b)\end{aligned} \tag{D1}$$

where $|\beta\rangle$ and $|\alpha\rangle$ are the ground and excited states for the two-level system with energy separation ω_a, a (b) is the annihilation operator the the cavity (mechanical) mode with frequency $\omega_c(\omega_m)$, G is TLS-cavity mode coupling strength, and g is optomechanical coupling strength. Following the process as described in references [42, 48], we write the system Hamiltonian in the diagonalized basis of the TLS-cavity Hamiltonian ($\mathbf{H}_{\rm JC}$). Restricting the number of photons in the cavity mode to one, the Hamiltonian $\mathbf{H}_{\rm JC}$ can be readily diagonalized such that $\mathbf{H}_{\rm JC}|\pm\rangle = \omega_\pm |\pm\rangle$ where

$$|+\rangle = \cos\theta\,|\alpha,0\rangle + \sin\theta\,|\beta,1\rangle \tag{D2a}$$

$$|-\rangle = -\sin\theta\,|\alpha,0\rangle + \cos\theta\,|\beta,1\rangle \tag{D2b}$$

$$\omega_\pm = \frac{\omega_a + \omega_c}{2} \pm \sqrt{G^2 + \frac{\Delta^2}{4}} \tag{D2c}$$

Here $\tan(2\theta) = 2G/\Delta$ and $\Delta = \omega_a - \omega_c$. The cavity annihilation operator in the restricted polariton basis can be written as $a \approx \sin\theta\,|\beta,0\rangle\langle+| + \cos\theta\,|\beta,0\rangle\langle-|$ [51] and the number operator as $a^\dagger a = \sin^2\theta\,|+\rangle\langle+| + \cos^2\theta\,|-\rangle\langle-| + \sin\theta\cos\theta(|+\rangle\langle-| + |-\rangle\langle+|) = 1/2\big(1 + \cos(2\theta)\sigma_z + \sin(2\theta)\sigma_x\big)$ where σ_x and σ_z are the Pauli matrices in the polariton basis. Substituting these relations in Eq. D1, the system Hamiltonian in the polariton basis becomes

$$\begin{aligned}\mathbf{H}_{\rm s} = &\,\omega_-\sigma_{--} + \omega_+\sigma_{++} + \omega_m b^\dagger b \\ &+ \frac{g}{2}\Big(\sin(2\theta)\sigma_x + \big(1 + \cos(2\theta)\sigma_z\big)\Big)(b + b^\dagger)\end{aligned} \tag{D3}$$

Replacing annihilation and creation operators by $b \to b - q_o/\sqrt{2}$ and $b^\dagger \to b^\dagger - q_o/\sqrt{2}$, where ($q_o = \sqrt{2}g/2\omega_m$) is the shift in the equilibrium position of the mechanical resonator in the polariton basis, the Hamiltonian becomes:

$$\begin{aligned}\mathbf{H}_{\rm s} = &\,\omega_-\sigma_{--} + \omega_+\sigma_{++} \\ &+ \frac{g}{2}\big(\sin(2\theta)\sigma_x + \cos(2\theta)\sigma_z\big)(b + b^\dagger) \\ &+ \frac{g^2}{2\omega_m}(\sin(2\theta)\sigma_x - \cos(2\theta)\sigma_z)\end{aligned} \tag{D4}$$

For a cavity-optomechanics system, we make the approximation that the optomechanical coupling strength is much smaller than the mechanical resonator frequency i.e. $g \ll \omega_m$ [42]. Using this approximation, we drop the terms with a factor of g^2/ω_m from the Hamiltonian. Further, we make the rotating wave approximation to neglect fast rotating terms from $\sigma_x(b + b^\dagger)$ to obtain a Jaynes-Cummings coupling between the polaritons and the mechanical resonator. Similar to the Hamiltonian presented in Eq (1), we add a coherent pumping at frequency ω_p to the lower polariton to obtain the following Hamiltonian:

$$\begin{aligned}\mathbf{H}_{\rm s} = &\,\Delta_1\sigma_{--} + (\Delta_1 + \Delta_2)\sigma_{++} + \omega_m b^\dagger b \\ &+ \frac{g}{2}\sin(2\theta)(b\sigma_{+-} + b^\dagger\sigma_{-+}) + \Omega(\sigma_{0-} + \sigma_{-0}) \\ &+ \frac{g}{2}\cos(2\theta)\sigma_z(b + b^\dagger)\end{aligned} \tag{D5}$$

where $\Delta_1 = \omega_- - \omega_p$, $\Delta_2 = \omega_+ - \omega_-$, σ_{+-} and σ_{-+} are the dipole operators for the polaritons, and $|0\rangle$ is the shorthand for $|\beta,0\rangle$. In the bad cavity regime, the lifetime of the cavity mode will be much smaller than the lifetime of the TLS. Therefore, the decay rates of the polariton states take the form [51]:

$$\begin{aligned}\gamma_+ &\approx \kappa\cos^2(\theta) \\ \gamma_- &\approx \kappa\sin^2(\theta)\end{aligned} \tag{D6}$$

Appendix E: Steady-state phonon number for the case $\gamma_1 = \gamma_2$

Solving the rate equations as in Appendix C by setting $\gamma_1 = \gamma_2$ for steady state phonon number gives:

$$\begin{aligned}\langle b^\dagger b\rangle = &\frac{\gamma_2\gamma n_{th}\Big(8\Omega^2(3g^4 + g^2\Omega^2 + 2\Omega^2) + \gamma_2^2(4g^4 + 20g^2\Omega^2 + 26\Omega^4) + \gamma_2^4(5g^2 + 11\Omega^2) + \gamma_2^6\Big)}{48g^2\Omega^4\gamma_2^2 + 6g^2\Omega^2\gamma_2^4 + \gamma\big(32g^4\Omega^2 + 16\Omega^6 + (1 + 2n_{th})\gamma_2^7\big)} \\ &+ \frac{2\Omega^2\gamma n_{th}\Big(2\gamma_2(6g^2\Omega^2 + 4\Omega^4) + \gamma_2^3(g^2 + 9\Omega^2) + \gamma_2^5\Big)}{48g^2\Omega^4\gamma_2^2 + 6g^2\Omega^2\gamma_2^4 + \gamma\big(32g^4\Omega^2 + 16\Omega^6 + (1 + 2n_{th})\gamma_2^7\big)}\end{aligned} \tag{E1}$$

Appendix F: A system of coupled cavities interacting with a mechanical mode

Following the reference [37] and the calculations in Appendix (D), the Hamiltonian for a system of coupled cavities interacting with a mechanical mode can be shown

to be equivalent to (D5). The following points should be noted to arrive at the result: 1) As the operators are linearized, restricting the maximum excitations to one for all three harmonic oscillators is valid. 2) Due to the weak coupling regime as pointed out by reference [37], the approximation $g/\omega_m \ll 1$ remains valid.

The coupled cavity system has been experimentally realized in the context of lasing action using coupled toroidal cavities out of which one supports a mechanical mode [49]. Consistent with the paper [37], we set the following parameters: $G = 10$ MHz (represents coupling strength between the two cavities here), $g = 0.05G, \omega_m = 2G, Q_m = \omega_m/\gamma = 10^5$ and an initial temperature of 300 mK corresponding to $n_{th} = 312$. Simulating the model using the quantum optics toolbox, we calculate variation of $\mathcal{F}$ with Ω and γ_2 (Figure 10). The minimum phonon number $\langle b^\dagger b\rangle_{min} = \mathcal{F}\times n_{th} \approx 0.235$ is obtained. Comparing this with [37], where the minimum phonon number $\langle b^\dagger b\rangle_{min} \approx 0.32$, is of the same order.

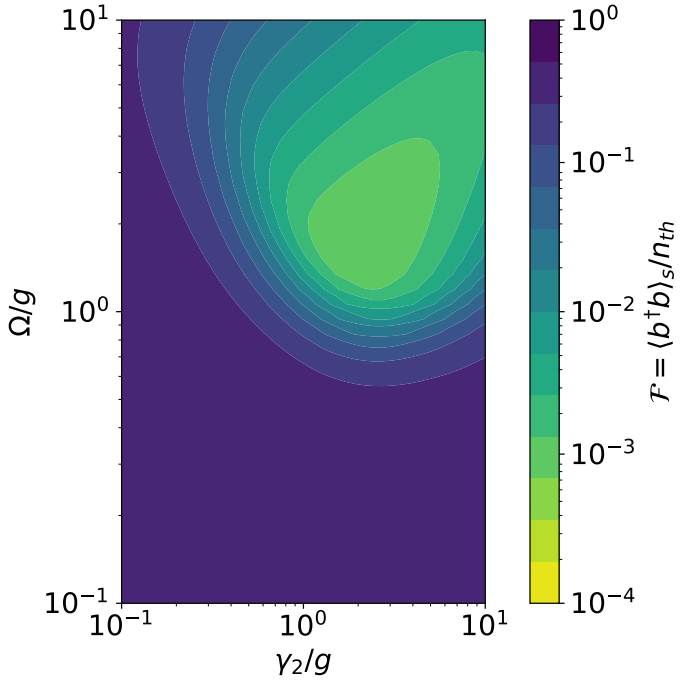

FIG. 10: Variation of steady state phonon number with Ω and γ_2 for coupled cavity system

Appendix G: Optimizing cooling for incoherent pumping

Following the reference [40], we set $\omega_m = 200$ MHz, $n_{th} \approx 200$, $g = 1$ MHz and $\Omega = 10g$. We plot the variation of $\mathcal{F}$ as a function of the phonon decay rate γ and the decay rate of the second excited state γ_2 in Figure 11. The white dot-dashed line represents the line $\gamma_2 = 2g$, the optimal decay rate obtained from analytical calculations. The results are in good agreement with the results obtained in [40] for the case of a single atom.

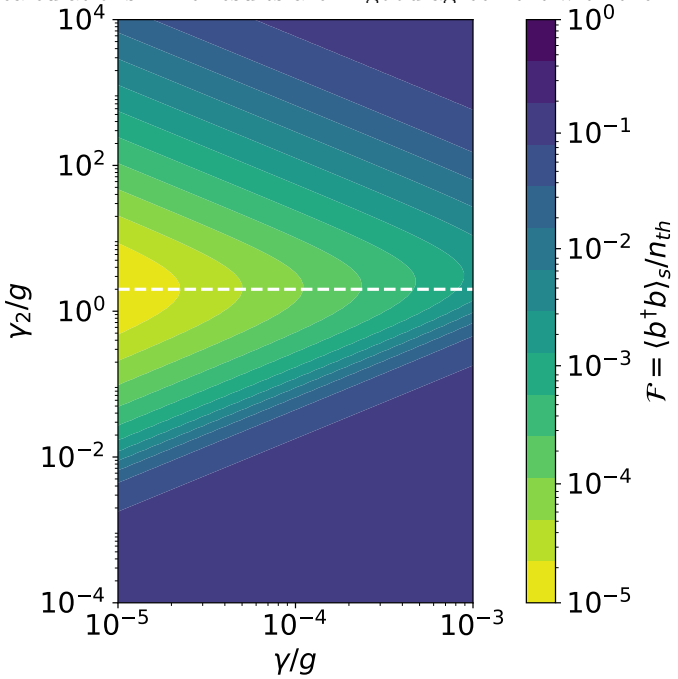

FIG. 11: Variation of $\mathcal{F}$ with the decay rate of second excited state γ_2 and phonon decay rate γ under incoherent pumping. The white dot-dashed line represents the optimal decay rate as obtained from our model. Here, $\omega_m = 200$ MHz, $n_{th} \approx 200$, $g = 1$ MHz and $\Omega = 10g$

[1] K. C. Schwab and M. L. Roukes, Putting mechanics into quantum mechanics, Physics Today **58**, 36 (2005).

[2] M. Aspelmeyer and K. Schwab, Focus on mechanical systems at the quantum limit, New Journal of Physics **10**, 095001 (2008).

[3] J. D. Teufel, T. Donner, M. A. Castellanos-Beltran, J. W. Harlow, and K. W. Lehnert, Nanomechanical motion measured with an imprecision below that at the standard quantum limit, Nature Nanotechnology **4**, 820 (2009).

[4] A. G. Krause, M. Winger, T. D. Blasius, Q. Lin, and O. Painter, A high-resolution microchip optomechanical accelerometer, Nature Photonics **6**, 768 (2012).

[5] Y.-W. Hu, Y.-F. Xiao, Y.-C. Liu, and Q. Gong, Optomechanical sensing with on-chip microcavities, Frontiers of Physics **8**, 475 (2013).

[6] T. P. Purdy, R. W. Peterson, and C. A. Regal, Observation of radiation pressure shot noise on a macroscopic object, Science **339**, 801 (2013).

[7] L. F. Buchmann, H. Jing, C. Raman, and P. Meystre, Optical control of a quantum rotor, Physical Review A **87** (2013).

[8] Y.-D. Wang and A. A. Clerk, Using interference for high fidelity quantum state transfer in optomechanics, Physical Review Letters **108** (2012).

[9] H. Wang, C. Dong, V. Fiore, and M. Kuzyk, Optomechanical dark mode, in *2013 Conference on Lasers & Electro-Optics Europe & International Quantum Electronics Conference CLEO EUROPE/IQEC* (IEEE, 2013).

[10] V. Fiore, Y. Yang, M. C. Kuzyk, R. Barbour, L. Tian, and H. Wang, Storing optical information as a mechanical excitation in a silica optomechanical resonator, Physical Review Letters **107** (2011).

[11] M. Schmidt, M. Ludwig, and F. Marquardt, Optomechanical circuits for nanomechanical continuous variable quantum state processing, New Journal of Physics **14**, 125005 (2012).

[12] K. Stannigel, P. Komar, S. J. M. Habraken, S. D. Bennett, M. D. Lukin, P. Zoller, and P. Rabl, Optomechanical quantum information processing with photons and phonons, Physical Review Letters **109** (2012).

[13] O. Romero-Isart, A. C. Pflanzer, F. Blaser, R. Kaltenbaek, N. Kiesel, M. Aspelmeyer, and J. I. Cirac, Large quantum superpositions and interference of massive nanometer-sized objects, Physical Review Letters **107** (2011).

[14] P. Sekatski, M. Aspelmeyer, and N. Sangouard, Macroscopic optomechanics from displaced single-photon entanglement, Physical Review Letters **112** (2014).

[15] B. Pepper, R. Ghobadi, E. Jeffrey, C. Simon, and D. Bouwmeester, Optomechanical superpositions via nested interferometry, Physical Review Letters **109** (2012).

[16] M. P. Blencowe, Effective field theory approach to gravitationally induced decoherence, Physical Review Letters **111** (2013).

[17] Y. long Liu, C. Wang, J. Zhang, and Y. xi Liu, Cavity optomechanics: Manipulating photons and phonons towards the single-photon strong coupling, Chinese Physics B **27**, 024204 (2018).

[18] C. Reinhardt, T. Müller, A. Bourassa, and J. C. Sankey, Erratum: Ultralow-noise SiN trampoline resonators for sensing and optomechanics [phys. rev. x 6 , 021001 (2016)], Physical Review X **7** (2017).

[19] R. Norte, J. Moura, and S. Gröblacher, Mechanical resonators for quantum optomechanics experiments at room temperature, Physical Review Letters **116** (2016).

[20] C. Genes, H. Ritsch, and D. Vitali, Micromechanical oscillator ground-state cooling via resonant intracavity optical gain or absorption, Phys. Rev. A **80**, 061803 (2009).

[21] C. Genes, H. Ritsch, M. Drewsen, and A. Dantan, Atom-membrane cooling and entanglement using cavity electromagnetically induced transparency, Phys. Rev. A **84**, 051801 (2011).

[22] F. Bariani, S. Singh, L. F. Buchmann, M. Vengalattore, and P. Meystre, Hybrid optomechanical cooling by atomic Λ systems, Phys. Rev. A **90**, 033838 (2014).

[23] X. Chen, Y.-C. Liu, P. Peng, Y. Zhi, and Y.-F. Xiao, Cooling of macroscopic mechanical resonators in hybrid atom-optomechanical systems, Phys. Rev. A **92**, 033841 (2015).

[24] Y.-D. Wang, Y. Li, F. Xue, C. Bruder, and K. Semba, Cooling a micromechanical resonator by quantum back-action from a noisy qubit, Phys. Rev. B **80**, 144508 (2009).

[25] Y. Li, L.-A. Wu, Y.-D. Wang, and L.-P. Yang, Nondeterministic ultrafast ground-state cooling of a mechanical resonator, Phys. Rev. B **84**, 094502 (2011).

[26] P. Zhang, Y. D. Wang, and C. P. Sun, Cooling mechanism for a nanomechanical resonator by periodic coupling to a cooper pair box, Phys. Rev. Lett. **95**, 097204 (2005).

[27] S. P. Tarabrin, H. Kaufer, F. Y. Khalili, R. Schnabel, and K. Hammerer, Anomalous dynamic backaction in interferometers, Phys. Rev. A **88**, 023809 (2013).

[28] T. Weiss and A. Nunnenkamp, Quantum limit of laser cooling in dispersively and dissipatively coupled optomechanical systems, Phys. Rev. A **88**, 023850 (2013).

[29] F. Elste, S. M. Girvin, and A. A. Clerk, Quantum noise interference and backaction cooling in cavity nanomechanics, Phys. Rev. Lett. **102**, 207209 (2009).

[30] A. Sawadsky, H. Kaufer, R. M. Nia, S. P. Tarabrin, F. Y. Khalili, K. Hammerer, and R. Schnabel, Observation of generalized optomechanical coupling and cooling on cavity resonance, Phys. Rev. Lett. **114**, 043601 (2015).

[31] Y.-C. Liu, Y.-F. Xiao, X. Luan, Q. Gong, and C. W. Wong, Coupled cavities for motional ground-state cooling and strong optomechanical coupling, Physical Review A **91** (2015).

[32] B. Sarma and A. K. Sarma, Ground-state cooling of micromechanical oscillators in the unresolved-sideband regime induced by a quantum well, Phys. Rev. A **93**, 033845 (2016).

[33] B. yuan Zhou and G. xiang Li, Ground-state cooling of a nanomechanical resonator via single-polariton optomechanics in a coupled quantum-dot-cavity system, Physical Review A **94** (2016).

[34] W. Zeng, W. Nie, L. Li, and A. Chen, Ground-state cooling of a mechanical oscillator in a hybrid optomechanical system including an atomic ensemble, Scientific Reports **7** (2017).

[35] Q. Mu, C. Lang, and P. Lin, Dynamic cooling of a micromechanical membrane in a double-cavity optomechanical system, International Journal of Theoretical Physics **59**, 454 (2019).

[36] Y.-L. Liu and Y. xi Liu, Energy-localization-enhanced ground-state cooling of a mechanical resonator from room temperature in optomechanics using a gain cavity, Physical Review A **96** (2017).

[37] Y. Guo, K. Li, W. Nie, and Y. Li, Electromagnetically-induced-transparency-like ground-state cooling in a double-cavity optomechanical system, Physical Review A **90** (2014).

[38] J. pei Zhu and G. xiang Li, Ground-state cooling of a mechanical resonator by single- and two-phonon processes, Journal of Applied Physics **111**, 033704 (2012).

[39] L. Li, R.-H. Luo, L. Liu, S. Zhang, and J.-Q. Zhang, Double-passage ground-state cooling induced by quantum interference in the hybrid optomechanical system, Scientific Reports **8** (2018).

[40] C. L. Cortes, M. Otten, and S. K. Gray, Ground-state cooling enabled by critical coupling and dark entangled states, Physical Review B **99** (2019).

[41] M. Khosla, S. Rao, and S. Gupta, Polarons explain luminescence behavior of colloidal quantum dots at low temperature, Scientific Reports **8** (2018).

[42] J. Restrepo, C. Ciuti, and I. Favero, Single-polariton optomechanics, Physical Review Letters **112** (2014).

[43] J. Johansson, P. Nation, and F. Nori, Qutip 2: A python framework for the dynamics of open quantum systems, Computer Physics Communications **184**, 1234 (2013).

[44] L. Biadala, Y. Louyer, P. Tamarat, and B. Lounis, Direct observation of the two lowest exciton zero-phonon lines in single CdSe/ZnS nanocrystals, Phys. Rev. Lett. **103**, 037404 (2009).

[45] C. Gautham, D. W. Snoke, A. Rastelli, and O. G. Schmidt, Time-resolved two-photon excitation of dark states in quantum dots, Applied Physics Letters **104**, 143114 (2014).

[46] Q. Lu, X. Chen, H. Yang, X. Wu, and S. Xie, Ultrahigh purcell factor, improved sensitivity, and enhanced optical force in dielectric bowtie whispering-gallery-mode resonators, IEEE Photonics Journal **9**, 1 (2017).

[47] J. Y. Lee, X. Lu, and Q. Lin, High-q silicon carbide photonic-crystal cavities, Applied Physics Letters **106**, 041106 (2015).

[48] J. Restrepo, I. Favero, and C. Ciuti, Fully coupled hybrid cavity optomechanics: Quantum interferences and correlations, Physical Review A **95** (2017).

[49] I. S. Grudinin, H. Lee, O. Painter, and K. J. Vahala, Phonon laser action in a tunable two-level system, Physical Review Letters **104** (2010).

[50] M. O. Scully and M. S. Zubairy, *Quantum Optics* (Cambridge University Press, Cambridge, England, 1997).

[51] T. Neuman and J. Aizpurua, Origin of the asymmetric light emission from molecular exciton-polaritons, Optica **5**, 1247 (2018).